View metadata, citation and similar papers at core.ac.uk brought to you by CORE
provided by Nottingham Trent Institutional Repository (IRep)

Submitted to Faraday Discussions: 24/04/18

Real-time *in situ* dynamic sub-surface imaging of multi-component electrodeposited films using *event mode* neutron reflectivity

A. Robert Hillman [1*], Robert Barker [2], Robert M. Dalgliesh [3], Virginia C. Ferreira [4], Emma J. R. Palin [1], Rachel M. Sapstead [1], Emma L. Smith [5], Nina-Juliane Steinke, [3] Karl S. Ryder [1] and Andrew D. Ballantyne [1]

[1] Materials Centre, Department of Chemistry, University of Leicester, University Road, Leicester LE1 7RH, UK.

[2] School of Physical Sciences, University of Kent, Canterbury, Kent, CT2 7NH, UK.

[3] Rutherford Appleton Lab, ISIS Facility, STFC, Harwell, OX11 0QX, UK.

[4] Centro de Química e Bioquímica, Faculdade de Ciências, Universidade de Lisboa, 1749-016 Lisbon, Portugal.

[5] Department of Chemistry, School of Science and Technology, Nottingham Trent University, Nottingham NG11 8NS, UK.

0000-0003-1868-5717 (Hillman)

0000-0002-4648-3461 (Ferreira)

0000-0001-5844-0883 (Smith)

0000-0003-2803-6884 (Ryder)

* Corresponding author; email: arh7@le.ac.uk

Abstract

Exquisite control of the electrodeposition of metal films and coatings is critical to a number of high technology and manufacturing industries, delivering functionality as diverse as anti-corrosion and anti-wear coatings, electronic device interconnects and energy storage. The frequent involvement of more than one metal motivates the capability to control, maintain and monitor spatial disposition of the component metals, whether as multilayers, alloys or composites. Here we investigate the deposition, evolution and dissolution of single and two-component metal layers involving Ag, Cu, and Sn on Au substrates immersed in the deep eutectic solvent (DES) Ethaline. During galvanostatically controlled stripping of the metals from two-component systems the potential signature in simultaneous thickness electrochemical potential (STEP) measurements provides identification of the dissolving metal; coulometric assay of deposition efficiency is an additional outcome. When combined with quartz crystal microbalance (QCM) frequency responses, the mass change:charge ratio provides oxidation state data; this is significant for Cu in the high chloride environment provided by Ethaline. The spatial distribution (solvent penetration and external roughness) of multiple components in bilayer systems is provided by specular neutron reflectivity (NR). Significantly, the use of recently established *event mode* capability shortens the observational timescale of the NR measurements by an order of magnitude, permitting dynamic *in situ* observations on practically useful timescales. Ag,Cu bilayers of *both* spatial configurations give identical STEP signatures indicating that, despite the extremely low layer porosity, thermodynamic constraints (rather than spatial accessibility) dictate reactivity; thus, surprisingly, Cu dissolves first in both instances. Sn penetrates the Au electrode on the timescale of deposition; this can be prevented by interposing a layer of either Ag or Cu.

Keywords: Electrodeposition; neutron reflectivity; bilayer; anodic stripping; copper; silver; tin

Introduction

Fabrication and control of sophisticated metal nano-architectures, layered structures and interfaces has become a necessary and integral feature of many contemporary core technologies. These include composite functional coatings for anti-corrosion and anti-wear applications in the automotive and aerospace industries, semiconductor device and chip production, electrochemically driven visual displays, energy storage in battery technologies as well as microelectronics assembly and printed circuit board (PCB) manufacture. [1, 2] In particular, PCB design and manufacturing processes are driven by the need to control the thickness, roughness and chemical composition of multi-layered metal structures at the nanometre scale. This is necessitated by technological and performance demands such as increased miniaturisation and power density (additionally requiring improved electrical and thermal conductivity).

Printed circuit board substrates are typically fabricated using copper conduction tracks but often utilise complex multi-layered structures deposited using additional metals such as Ni, Pd, Sn, Ag and Au (four of these elements feature in the present study). Copper, whist having very good electrical and thermal properties, oxidises rapidly in air passivating the surface to subsequent assembly processes such as component bonding. Coatings of Ag and Au (50 – 100 nm) are often applied to Cu in order to protect the surface but the stability of these coatings is limited by the solid-state mixing of Cu and Ag or Au atoms at the interface. This can lead to further surface passivation or the formation of intermetallic phases that introduce mechanical weakness in assembled devices. For, example the formation of Cu-Sn intermetallic phases over the 100 nm distance scale (perpendicular to the plane of the interface) in solder joints is known to increase the instance of brittle fracture in component joins leading to the early failure of consumer electronic devices (*e.g.* phones, computers and related mobile devices). [3] Consequently, there is a range of sophisticated and complex multi-layer structures, for example involving Cu/Ni/Au and Cu/Ni/Pd/Au, that have been developed to reduce inter-diffusion of metals, minimise substrate oxidation during storage and improve bonding interactions for component assembly processes such as surface mount soldering or gold-wire bonding. Additionally, the control and minimisation of surface roughness at metal-metal layered PCB interfaces can be critical in determining the performance of devices at high frequency (*e.g.* high bandwidth data communications). Here

a rough interface results in very long signal path (leading to signal loss) because of the high-frequency "skin effect".

The layered structures are most often fabricated using electrochemical deposition and the overwhelming majority of electrolytic metal processing is carried out in water-based solutions. In PCB manufacturing a range of such electroplating and fabrication methods are covered under the general description of a Damascene process. [4] However, despite their abundance and the historical time scale over which they have been developed, aqueous electrochemical deposition processes still possess significant limitations such as low current efficiency, coating embrittlement and dendrite formation. Stringent process control is often necessary to maintain specification; this leads to plating bath complexity and rigorous maintenance requirements. [5] In addition, strong inorganic acids and bases are often needed and the metal salts required, notably cyanides, are often very toxic. As a result, the use of novel ionic liquid [6] (IL) media and in particular deep eutectic solvents [7] (DES) is becoming increasingly attractive.

DESs are systems formed from eutectic mixtures of Brønsted or Lewis acids and bases, typically mixtures of the salt choline chloride with small hydrogen bonding molecules such as ethylene glycol or urea. [7] DES based electrolytes have been used for the electrodeposition of a wide range of metal and alloy coatings including Cu, [8, 9] Sn, [10, 11, 12] Zn, [13, 14] Cr, [15, 16] Zn/Ni [17] and Zn/Sn. [18] These DES electrolyte media offer prospective improvements in process control/efficiency, environmental sustainability/impact and functionality as well as giving access to reactive metal deposition not previously possible (for example Al). However, due to the fundamental differences between molecular solvents like water and ILs/DESs there are significant disparities in the way metal films nucleate and grow on surfaces. [19] This presents intellectual and practical challenges in order to be able to understand and control the coating processes and exploit the potential benefits of these media.

We have been engaged in the study of electrolytic metal deposition and dissolution in DES media, with particular relation to potential applications in the electronics manufacturing sectors. [20] Here it is important to be able to control and predict rate of deposition of the metal as well as to achieve target values of surface roughness and coherent, dense coatings. Monitoring surface roughness, film thickness (both at the nanometre scale) and density

during electrodeposition can be achieved by a combination of techniques including electro-gravimetry (Quartz Crystal Microbalance, QCM) [21], holographic imaging (Digital Holographic Microscopy, DHM) [22], scanning electron microscopy (SEM), optical profiling [23] and scanning probe microscopy (Atomic Force Microscopy, AFM) [24] as well as integrated electrochemical techniques (chronocoulometry). Whilst each of these techniques has individual strengths, in isolation none can deliver all of the necessary insights and metrology. Electrochemical and QCM measurements have good temporal resolution but are averaged over the sample volume (both across the surface and throughout its depth). Optical microscopy is limited by line of sight access to the electrified interface and the spatial resolution of visible wavelengths, whereas high resolution imaging techniques such as SEM can only be utilised *ex-situ*. Probe microscopy can offer great insight into the shape of an evolving surface during growth [25] and into the mechanism of growth, but the proximity of the sharp probe close to the electroactive interface, or touching it, can initiate nucleation events and thus perturb the measurement. Furthermore, none of these techniques is capable of quantifying the internal composition of the deposited film during deposition.

An alternative is to use neutron reflectivity (NR) techniques. [26] This approach has many similarities to optical ellipsometry – and indeed the mathematical considerations are similar – but NR has three major advantages in this context. First, the metal coatings here are relatively transparent to neutrons, but are optically opaque so ellipsometry is unable to penetrate to their interior. Second, for the neutron sources available, the effective wavelength scales at which measurements can be made are in the (sub)nanometre range. Third, neutrons interact with the nuclei (*cf.* photons interact with the electrons) in the system, so NR is isotopically sensitive. Since the films and solution used here are strongly contrasted from a neutron perspective, this last attribute was not required, but (see below) we have used this to good effect elsewhere.

Thus, neutron reflectivity techniques are able to provide not only thickness and roughness data for growing films but also compositional detail perpendicular to the plane of the electrode, *i.e.* in the direction of growth. Development of NR methods to study “buried” interfaces under electrochemical control has distinguished composite and bilayer polymer films, [27] revealed permeating solvent in electroactive polymer [28] and metal hydroxide [29] films, identified permselectivity failure at high electrolyte concentration, [30] and revealed 1D

profiling of diffusion and reaction within a film of a solution phase mediator. [31] Of relevance here, we have used a combination of *in-situ* techniques including NR to evaluate the influence of electrolytic deposition conditions on the solvation of reactive conducting polymers. [32, 33] More recently we have studied the real time deposition of Cu and Ag metals on a gold electrode using real-time electrochemical event mode NR methods. This has revealed new insights into the progression of film thickness, roughness and solvation as a function of electrochemical methodology and deposition rate for the single metal systems that inform the studies reported here. [34]

Historically, the primary disadvantage of NR as compared to ellipsometry has been time resolution. Dependent on the system (notably substrate/layer/solution contrast), acquisition times on the order of hours for a single reflectivity profile were not uncommon. Thus, from an electrochemical perspective, NR was a static technique. More subtly, the manner in which data were acquired was such that one had to make a decision on time resolution ahead of the experiment; this made the experiment instrumentally expensive and interpretation problematic. The recent establishment of *event mode* data acquisition resolves this issue. Expressed simplistically (though technically complex) the instrumentation captures every neutron event (with an individual time stamp). One can then make reversible decisions regarding data averaging post-experiment, thereby optimising signal-to-noise and temporal resolution. Together with enhanced detection, this now permits us to achieve good signal to noise in the NR data at temporal resolution of typically 5-10 minutes (according to physical conditions).

In addition to the NR methods, we have used galvanostatic (chronopotentiometric) stripping techniques (also known by the acronym of STEP, *s*imultaneous *t*hickness *e*lectrochemical *p*otential) [35, 36] and QCM gravimetric analysis to study the deposition, ageing and stripping of bi-metallic coatings deposited from DES media. In doing so we have sought to gain new insights into the developing thickness, interfacial roughness and transitional composition of the metal-metal interfaces at the nanometre scale. These insights will contribute to the design and implementation of new environmentally sustainable, high efficiency (materials and energy) processes for control of metallic interfaces in PCB manufacture.

Ultimately our goal is the detailed spatio-temporal characterization of multi-component systems involving reactive and/or spatially mobile metal(s). In previous work [34] we have

used the recent NR developments described above to characterise the growth and dissolution of *single* component metal films. Our generic goal here is to extend this to more complex (bi-)layer films applied to a Au electrode by electroplating in DES medium comprising a mixture of ethylene glycol (Eg) and choline chloride (ChCl) in a stoichiometric ratio 2:1 (2Eg:1ChCl). This DES electrolyte is available commercially under the registered name of *Ethaline*. Specific objectives are, under dynamic *in situ* conditions, determination of the thickness, solvent content, roughness and inter-penetration (with each other and the Au substrate) of Ag, Cu and Sn films, and the variations of these parameters during metal deposition and dissolution.

Experimental

Reagents and materials

All chemicals were used as received. Copper (II) chloride, tin (II) chloride and silver chloride were supplied by Acros Organics. Choline chloride (ChCl), ethylene glycol (EG) and (3-mercaptopropyl) trimethoxysilane (MPTS) were supplied by Sigma Aldrich. Ethaline was synthesised from a 2:1 molar ratio of ethylene glycol to choline chloride. The mixture was stirred at 70 °C until a clear, homogeneous solution was observed. Metal chloride solutions (10 mM or 20 mM in Ethaline 200; see individual figure legends) were prepared by stirring at 50 °C until dissolved and continued stirring upon cooling to avoid crystal formation.

For QCM experiments, 5 mm diameter Au coated quartz crystals were used as working electrodes. For STEP experiments, Au coated glass microscope slides were used as working electrodes (exposed electrode area *ca.* 2 cm^2). For NR and STEP experiments, the Au-coated quartz working electrode was prepared by coating the quartz/glass with a monolayer of MPTS. A sulphur-containing binding layer was used (as described previously [34]) to ensure that the Au did not delaminate from the quartz. Finally, a Au layer was sputter coated onto the MPTS binding layer to a thickness of ca. 20–30 nm. In the case of all electrochemical experiments, a Ag wire quasi reference electrode was used; in the high chloride activity environment of Ethaline, this has proved to adopt a reproducible potential. [34] A TiO_2 coated Pt mesh was the counter electrode in a standard three-electrode cell configuration. For NR experiments, a purpose built electrochemical cell was used, [31,32] whereby the Au-coated quartz block acted as the working electrode. This configuration (shown in Fig. 1) has been

demonstrated to permit NR measurements with effective electrochemical control of metal deposition from DES media. [34]

Instrumentation

NR measurements were performed at room temperature on OFFSPEC at the ISIS neutron and muon source at the Rutherford Appleton Laboratory (Harwell, Oxford, UK). All measurements were carried out in event mode. Data were 'time sliced' into sections post-experiment and exported to the fitting software (see below). The data were sliced into 500 s 'sections' for deposition experiments and 250 s sections for dissolution. An incident angle (θ) of 0.5° and a λ range of 1.0–14 Å were used, giving a useable momentum transfer (Q) range of $0.008 < Q$ / Å^{-1} < 0.07. The neutron beam footprint was constrained to lie within the cell dimensions giving an effective instrumental resolution of ΔQ / Q ~2 %. The cell volume was 25 cm ^{3}. The start of each electrochemical experiment was triggered by the neutron instrument. Electrochemical/neutron data were recorded simultaneously. All electrochemical experiments were carried out using an IVIUM CompactStat potentiostat controlled by IviumSoft software version 2.224. All EQCM experiments were carried out using a Seiko EG&G QCM922A unit controlled using an analogue output to IviumSoft v. 2.224 software. Admittance spectra were recorded using the Sekio QCMAdm macro (QCM922A Admittance Data Acquisitionrevision 2.1.0.0) within Microsoft Excel.

Electrochemical procedures

Potentiostatic measurements**.** For STEP experiments, copper (10 or 20 mM $CuCl_2$), silver (10 mM AgCl) and tin (10 or 20 mM $SnCl_2$) in Ethaline were deposited potentiostatically onto the Au-coated glass working electrode. Deposition experiments using 10 mM metal chloride were carried out for 7.2 x 10^3 s (2 h) and those using 20 mM for 3.6 x 10^3 s (1 h.) A higher concentration of metal chloride was used in selected cases to bring the experimental timescale into a convenient range. Unless otherwise stated, Ag was deposited at -0.1 V, Cu at -0.6 V and Sn at -0.5 V. For the CuAg experiment, Ag was deposited at -0.4 V so as to avoid dissolution of the underlying Cu layer.

For EQCM experiments, copper (20 mM $CuCl_2$) and silver (20 mM AgCl) were deposited potentiostatically onto a 0.5 cm diameter Au electrode on an AT-cut QCM crystal (f_0 = 9

MHz). For all experiments, Ag was deposited at -0.1 V for 1.8 x 10^3 s (0.5 h) and Cu at -0.6 V for the same length of time.

For neutron reflectivity experiments, copper (10 mM $CuCl_2$), silver (10 mM AgCl) and tin (10 mM $SnCl_2$) in Ethaline were deposited potentiostatically onto the Au coated quartz working electrode, with an exposed electrode area of ca. 28 cm^2. Ag was deposited first at −0.4 V for 7.2 ×10^3 s (2 h) and Cu was deposited on top of the Ag layer at −0.4 V for 10.8 × 10^3 s (3 h) and the resulting i vs. t traces were recorded. For the Sn deposition experiment, Sn was deposited at -0.4 V for 21.6 x 10^3 s (6 h.) For NR experiments, <10% of the metal ion salt dissolved in solution was deposited in each case; there is no substantive depletion of solution phase metal ion reactant. The electrochemical cell for NR measurements was assembled using Dow Corning (3145 RTV-Clear MIL-A-46146) adhesive sealant.

Galvanostatic measurements (STEP stripping). All dissolution experiments were carried out galvanostatically in fresh Ethaline electrolyte at room temperature, using the same electrode configuration as for the deposition experiments. Current density values are detailed in figure legends for specific experiments.

NR data fitting/analysis

We have recently described the relevant aspects of NR data interpretation for systems of this type. [34] In summary, all data fitting was carried out using RasCal, functioning as a script within Matlab.[37] This software uses iterative fitting procedures within multi-parameter models. The outcome of the fitting process is a scattering length density (SLD) profile which, through the known scattering lengths of the constituent atoms, is a measure of their relative population, *i.e.* the spatial profile of atomic composition. [26] Data fitting errors were determined using a "bootstrap" error analysis function within RasCal. [38]

Results

Overview

Ultimately, the intent is to explore the spatial structure and dynamics of complex multicomponent systems. To accomplish this we need to move stepwise, commencing with notionally simple single component systems and progressively introducing the structural and (electro)chemical complications. In a previous study, we used NR to follow the dynamics of copper and silver electrodeposition and dissolution (stripping) in *single*

component systems.[34] Our first advance here is therefore to extend consideration to *two* component Ag/Cu bilayer systems on Au: we consider both configurations, *i.e.* Au/Ag/Cu and Au/Cu/Ag. From our previous study, we know that neither of these individual systems interacts with the Au substrate (on the timescale of the measurements), so the second advance is to consider the deposition of a metal (Sn) that *does* interact with the Au substrate (on the timescale of the measurements). Thirdly, we include the reactive metal in a bilayer system, with either Ag or Cu.

In summary, we wish to consider one- and two-component systems, each of which may or may not involve a reactive or spatially mobile metal. Of the four combinations, we previously considered one-component systems that do not involve a reactive/mobile metal. Here we explore the remaining three combinations: two-component non-reactive bilayers (Ag/Cu in both configurations); a one-component reactive system (Sn on Au); and two-component systems involving a reactive metal (Ag/Sn and Cu/Sn on Au). Methodologically, we use the electrochemical potential (whether as the control function or response) to delineate the reacting species, nanogravimetric measurements to assay the process, and NR to provide insight into the structures of depositing and dissolving (bi-)layers.

Silver/copper bilayer (Au[electrode]/Ag/Cu)

Au/Ag/Cu layers were formed by separate potentiostatic deposition of Ag then Cu from Ethaline solutions (see Experimental and figure legends, below, for details). We note that the Cu oxidation state in the bulk Ethaline solution is Cu(II); in practice, in this ca. 5 mol dm^{-3} chloride solution it will be present as a chloro complex. This contrasts with the stripping part of the experiment (see potential response, below), the nature of which is such that dissolution will initially generate a Cu(I) species (again as a chloro complex).

In this simplest of bilayer configurations, which we use to establish methodology, the expectation is that galvanostatic stripping (passage of anodic current) will initially result in dissolution of the Cu. This is expected on the grounds that (i) the Cu(I/0) redox potential is more negative than that of the Ag(I/0) redox potential and (ii) Cu is exposed to the solution while Ag is not. In other words, both thermodynamics and spatial accessibility predict the dissolution sequence *Cu, then Ag.*

The experimental data for this situation are shown in Fig. 2. Qualitatively, the predictions of the previous paragraph are borne out. Quantitatively, the potential responses in this galvanostatically controlled experiment are consistent with the Cu(I/0) couple for the first ca. 3000 s then, when all the Cu is consumed, with the Ag(I/0) couple for the subsequent ca. 4000 s. After this time, the potential rises sharply and the Au electrode is progressively dissolved. The absence of a response (plateau) at potentials different to those associated with the elemental metals signals the absence of intermetallic phases.

The timescales involved, which effectively represent charge in the galvanostatic experiment, support this interpretation. The charge associated with Ag dissolution is 96% of that associated with deposition; we attribute this to minor departure from perfect deposition efficiency. The charge associated with the copper dissolution is a little less than half of that associated with the prior deposition step. This is a combination of a 2e deposition process with a deposition efficiency of ca. 70% and a 1e dissolution process; the low deposition efficiency, which is slightly variable from experiment to experiment, is attributed to the greater prominence of parasitic currents in this deliberately low current density format).

Having established speciation, we move to continuous assay of the dissolution process using the EQCM (see Fig. 3). Fig. 3a shows the admittance spectra of the resonator system *ex situ* (*i.e.* in air) at key points in the EQCM experiment: prior to deposition, after Ag deposition, after Ag and Cu deposition, and after stripping both Cu and Ag. In this case, since the Au layer on the quartz resonator is very thin, care was taken to avoid entering the “Au dissolution” zone at the end of the stripping experiment (see annotation of Fig. 2). Thus, the start and end spectra in Fig. 3a are indistinguishable. The high Q-factors ($1.7\text{-}2.0 \times 10^4$) throughout this experiment are typical for rigidly coupled films. Fig. 3b shows the corresponding spectra *in situ*. The qualitative trends and return to original response are analogous to those in Fig. 3b. The Q-factors are decreased to ca. 3.6×10^2, consistent with the high viscosity DES medium, but the independence of Q-factor with surface composition/configuration supports use of the Sauerbrey equation for interpretation of the deposition/dissolution processes.

The frequency response, interpreted gravimetrically (see above), *during* the bilayer stripping experiment is shown in Fig. 3c. To facilitate correlation of the speciation (potential) and assay (mass) data, the gravimetric response is overlaid on the potential response (analogous

to Fig. 2). The immediately striking feature is the abrupt change in gravimetric response at the point in time at which the potential response signals a shift from Cu to Ag dissolution; this is the nanoscale analog of the classical Faraday experiment, but in reverse mode in a multi-component system.

There are two other points of note arising from the data in this figure. First, the time interval (and thus charge) associated with the Cu dissolution indicates a prior deposition efficiency of 89%. Second, although care was taken to avoid the potential rising sufficiently high as to drive Au dissolution, there is the beginning of another process at the end of the experiment ($t \approx 1800$ s). Based on the potential, we interpret there to be further oxidation of the dissolved copper, i.e. reaction of the Cu(II/I) couple.

NR data for the processes of Figs. 2 and 3 are shown in Fig. 4. Qualitatively, in both panels a and b one can see the presence of fringes, the period of which (in momentum transfer) *decreases* progressively with time. Given that momentum transfer represents inverse space, this signals a progressive *increase* in film thickness. The fact that the fringes are clearly visible, i.e. not damped, suggests that the interfaces involved are relatively sharp (low roughness). Naturally, the Ag deposition data is essentially the same as previously described, [34] since at this point it is a single metal layer. Interpretation of the data for overlaying of the Cu deposit, primarily in terms of distinguishing a bilayer from an intermetallic phase or interpenetrating network, requires further analysis (below). The final panel in Fig. 4 shows the sequence of NR profiles found as the metals are galvanostatically stripped (analogous to the experiment of Fig. 2). Here, there is much less evidence of fringes, suggesting that dissolution does not proceed by means of a progressive spatially uniform retreat of the Cu/DES interface.

The outcomes of the fitting of the R(Q) profiles of Fig. 4 are shown in Fig. 5a for deposition of the Ag and Cu (presented as though continuous in time within a single experiment) and in Fig. 5b for the dissolution. Looking at Fig. 5a, at $t = 0$ and moving from left to right along the distance axis (perpendicular to the interface) we see scattering length density (SLD; see above) values representative of the underlying quartz, then the MPTS bonding layer (the "dip" in SLD), then the Au, with a diffuse (rough) interface to the electrolyte. With increasing time (moving backwards in the diagram), there is the progressive growth of an external layer identified on the basis of SLD (see below) as Ag; this growing layer has a diffuse

interface with the electrolyte. In the second half of the deposition (from t ≈ 18000 s), there is the growth of a second layer of higher SLD (consistent with that of Cu), again with a rough exterior.

These observations are quantified in Tables 1 and 2, for Ag and Cu deposition, respectively. In Table 1, the scattering length density is, within experimental uncertainty, that for pure Ag, *i.e.* an apparently (see below) compact pore-free film. The roughness of the growing layer, as sampled, does not change with time; the mean value of the roughness is 58.9 (±3.3) Å, replicating that of the Au substrate. The situation for the Cu layer is somewhat different, in that the SLD for the layer is systematically (though not dramatically) below the value for a pure compact Cu layer (6.54 x 10^{-6} $Å^{-2}$); the implication is a small amount of porosity. Additionally, the roughness of the Cu layer increases progressively from a value typical of the Ag underlayer to a value that is ca. 50% greater.

Turning to the fitted dissolution data, the qualitative picture (see Fig. 5b) is that the reverse sequence for "Ag deposition, Cu deposition" is "Cu stripping, Ag stripping". Quantitatively (see Tables 3 and 4), the picture is a little more nuanced, in that the roughness of the dissolving Cu layer is always significantly greater than for the depositing bilayer; there is some scatter, but the mean value is 120 Å. In the last few sampled time slices, the roughness of the layer is on the order of (and ultimately greater than) the fitted film thickness. We interpret this to indicate that, during the later stages of Cu stripping, the "layer" is in fact a collection of Cu islands on the Ag underlayer; the model used is not designed to represent this physical situation. During the Ag stripping, the mean roughness is 90 Å, somewhat greater than during Ag deposition (see above). The SLD for the Cu layer indicates the presence of a small amount of solvent even during the early stages; we return to layer porosity later.

Copper/silver bilayer (Au[electrode]/Cu/Ag)

We now move to the spatial inverse of the system discussed in the previous section, i.e. a Cu/Ag bilayer on Au, with Cu (Ag) as the inner (outer) layer. The process (sequential potentiostatic deposition) for fabrication of these structures was analogous to that described above, with the exception of the order. We thus proceed immediately to the STEP experiment (see Fig. 6) in which the metals are galvanostatically stripped. Given that,

notionally, only the Ag (outer) layer is exposed to the electrolyte, the expectation is that we would see Ag stripping (at E $\approx$ 0.1 V) then, after removal of all the Ag, stripping of the exposed Cu (at E $\approx$ -0.1 V). This is *not* what is observed. In fact, the STEP E(t) signature is for all practical purposes the same as for the Au/Ag/Cu structure of Fig. 2. Expressed differently, the anticipated spatial control is not exhibited. We deduce that the Ag deposit contains sufficient pinholes to permit Cu access to the electrolyte, such that the Cu is the first layer (controlled by thermodynamic conditions) to dissolve. It is clear that a relatively small number of nanoscale imperfections in the Ag layer are sufficient, since (see Table 1) we are able to deposit Ag with immeasurably low (in practice < 1%) solvent content. Given the similarity of responses in Fig. 2 and Fig. 6 (in both cases taken all the way through to Au dissolution), we do not repeat the STEP potential response arguments given above.

The corresponding EQCM responses are shown in Fig. 7; as before, since the Au substrate electrode in this experiment is relatively thin, we arrest the experiment before Au dissolution commences. The Q-factors for the resonator in air prior to and at the end of the experiment (bare Au) and after deposition of Ag then Cu are all high (1.7-2.0 x 10^4). Viscous phenomena upon immersion in the DES damp and broaden the resonances (Q-factors decrease to 3.4-3.6 x 10^2), but the independence of Q-factor from the presence of surface layer(s) permits simple gravimetric interpretation of the frequency response.

The overlaid mass (frequency) and potential responses to stripping are shown in fig. 7c. As for the Au/Ag/Cu system (Fig. 3c), we see first Cu stripping, then synchronised abrupt changes in the potential and mass responses (at t $\approx$ 358 s) to a Ag(I/0) dictated response. At longer times (t $\approx$ 1350 s) there is the same appearance as in Fig. 3 of Cu(I) oxidation. We attribute the absence of this in the experiment of Fig. 6 (or the counterpart for the inverse bilayer in Fig. 2) to the difference in timescales (dictated by the combination of Ag layer thickness and current density): in the case of Fig. 7c, the timescale is rather shorter, so the Cu(I) has had less time to diffuse away from the surface.

Tin single layer (Au[electrode]/Sn)

We now introduce the chemical complexity of a reactive metal, i.e. one that interacts with the Au substrate. We start with a single layer (notionally) of Sn potentiostatically deposited on Au. The STEP experiment potential response for the attempted galvanostatic stripping of

Sn is shown in Fig. 8. Were there no interaction between the Sn and Au, one would expect to see a single wave with the plateau centred at $E \approx -0.4$ V. In fact, we see a series of at least four discernible waves before the potential rises to a value typical of Au dissolution (see annotation of Fig. 2). The implication is formation of a range of AuSn intermetallic phases.

The experiment of Fig. 8 involved a Au thin film electrode deposited on a glass slide. This permitted visual inspection of the "dry" side of the electrode (Au/glass interface). Prior to Sn deposition, the colour of the electrode was (obviously) gold, but after Sn deposition *both* sides of the electrode showed clear visual evidence of the presence of tin. Assuming the Au electrode (thickness, $h_{Au} \approx 200$ Å) to be homogeneous and pinhole-free and taking the timescale to be that of the deposition process (t= 7200 s), it is possible to estimate the diffusion coefficient for Sn atoms through Au to be on the order of 10^{-15} cm^2 s^{-1}.

Fig. 9 shows NR profile acquired during the deposition of Sn on Au. In contrast to the data for the Ag and Cu systems, both individually (here in the context of generating bilayers and as reported elsewhere in the context of single layers [34]) and as one component of a completed bilayer, we do *not* see the formation and evolution of fringes. Both the deposition and stripping electrochemical responses (current in the former case and potential in the latter case; see Fig. 8) unambiguously signal the growth of a Sn layer, but the NR data show this not to be as spatially segregated layer. At this time, we have not been able to fit the evolving NR profiles. The indication is that the Au,Sn layer is a structurally complex composite, with multiple phases (see Fig. 8) whose spatial and temporal distribution is governed by a combination of homogenous diffusion and possibly more rapid Sn transport through imperfections (*e.g.* pinholes). The absence of clear fringes suggests that the layer is relatively rough compared to the Au substrate.

Silver/tin and copper/tin bilayers (Au[electrode]/Cu/Ag and Au[electrode]/Cu/Sn)

The observations of the previous sections demonstrate that, under the conditions and on the timescales of the experiments described here, (i) both Ag and Cu layers maintain their integrity with respect to each other and to the Au substrate, and (ii) Sn penetrates Au thin film electrodes. Combining these two facts, we sought to determine whether prior deposition of Ag or Cu on Au would create a barrier layer to subsequently deposited Sn. We therefore present data, based on the STEP experiment, as a test of this hypothesis.

Fig. 10 shows the potential response in a STEP experiment for what is notionally a Ag/Sn bilayer on Au. The response is reminiscent of that seen for the Ag/Cu bilayer (Fig. 2). The more electronegative element (Sn), which is the component exposed to the solution, is stripped first; thermodynamics and spatial accessibility operate in unison. When the Ag is fully dissolved, the potential shifts abruptly to a value consistent with Au dissolution. This last point allows us to assign charges (readily derived from timescale in this galvanostatic experiment) to the processes assigned to Sn and Ag stripping. For Sn deposition and dissolution, respectively, the charges are 0.350 C and 0.099 C. We attribute this largely to low Sn deposition efficiency as a consequence of the low current density format, designed to optimise the NR experiment but in which low level background/parasitic currents that are ordinarily insignificant accumulate to make a significant contribution to the charge; in a more conventional electroplating configuration we achieve a deposition efficiency of ca. 95% [39] so the issue here is not reagent-based. For Ag deposition and dissolution, respectively, the charges are 0.231 C and 0.246 C. We interpret this to indicate essentially 100% deposition efficiency, and perhaps a small component of the Sn dissolution within the assayed interval.

Fig. 11 shows the analogous potential response in a STEP experiment for what is notionally a Cu/Sn bilayer on Au. The closeness of the Sn and Cu standard electrode potentials means that the shift between the two plateaux is less dramatic, but their presence is unambiguous. Thus, as in Fig. 10, thermodynamics and spatial accessibility operate in unison, so Sn is stripped first. The Cu response is complicated by the fact that it occurs last, so there is an opportunity for both Cu(0) (from the surface) and Cu(I) (from the solution) oxidations to take place (see response at $t \approx 4500$ s) before Au dissolution ultimately occurs. Based on the coulometric data, the Sn deposition efficiency is ca. 50%.

Discussion

The observations of the previous section are made possible by the substantially improved time resolution and interpretation regime offered by event mode data acquisition; this has not yet been widely exploited. In broad terms, the improvement in time resolution is approximately an order of magnitude, which brings the NR experiment into the time frame of the STEP and (E)QCM experiments. Each of these experiments has a distinct focus – metal

identification (STEP), gravimetric assay (QCM) and spatial distribution of components (NR) – and a significant methodological accomplishment is that we are able to link the data.

The STEP experiment has proved to be a powerful diagnostic in the identification of dissolving species (*reactant*, in a stripping experiment): it distinguishes individual metals from intermetallics and, in the former case, provides unambiguous identification. Moving to the *product* that is released to solution, the gravimetric data from the QCM (*via* mass/charge ratio) indicate the change in oxidation state. While this is trivial in the case of Ag, it is an important question for metals with multiple stable oxidation states, exemplified here by Cu, but very common amongst transition metals.

For two-component systems (simplistically bilayers), the sequence of dissolution is influenced by two factors: standard electrode potential and exposure to the electrolyte. The former represents the thermodynamic driving force and the latter may be considered as a steric effect. Irrespective of the reactivity of a metal, if it is not exposed to the electrolyte it cannot dissolve; surface protection against corrosion exploits this concept. With this in mind, it is surprising that a Cu inner layer in a Cu/Ag bilayer dissolves first, despite the presence of a Ag overlayer. This has significant implications for the application of these electrolyte media to the production of coatings for electronic devices. The NR data show the Ag layer to be dense and to have very low solvent (void) volume fraction, typically <1%. We deduce that even small pinholes provide effective pathways for Cu/electrolyte contact. Specular NR measurements (as here) provide high spatial resolution perpendicular to the interface, but average the composition laterally. In order to make the distinction between lateral and vertical processes, off-specular NR measurements, which provide in-plane structure, would be valuable.

Conclusions

We conclude that *event mode* capture of synchronous neutron scattering events during electrochemical growth is a powerful means of enabling time-resolved measurements of the composition profiles of growing and dissolving metal films. When this information is combined with the outcomes of electrochemical STEP and gravimetric QCM observations, it is possible to assemble a detailed picture of the species involved, their populations and their spatial dispositions on the nanoscale at advancing or receding metal/electrolyte interfaces. Exploitation of this capability has enabled accomplishment of our generic goal of

characterising the growth and dissolution of metal films comprising two metal components, one of which may be reactive or mobile.

Turning to the specific objectives, we have determined *in situ* under dynamic conditions the thickness, solvent content, roughness and inter-penetration (with each other and the Au substrate) of Ag, Cu and Sn films during metal deposition and dissolution in Ethaline medium. Amongst this set, the only instance in which we find interpenetration (on the timescale of the experiments conducted) is of Sn into the Au electrode; interposing a Ag or Cu layer between the two prevents this.

Sequentially deposited Ag,Cu layers of either configuration comprise segregated layers. During deposition, their solvent content is very low and their external roughness is not dramatically different to that of the underlying Au substrate. Sequential stripping is governed by thermodynamic considerations: even the very low level (<1%) of pinholes in an outer Ag layer of a Cu/Ag bilayer is sufficient to permit Cu dissolution prior to Ag dissolution.

To date, a full description of Sn penetration into Au has not been accomplished. By analogy with Cu dissolution through pinholed Ag, we suspect that Sn entry into Au may be facilitated by pinholes. The resulting combination of lateral and vertical diffusional processes requires more sophisticated modelling.

In addition, we identify three other aspects for future study. First, there is the obvious opportunity that event mode NR data acquisition offers for extension to a wider portfolio of metal systems. In the context of electronic applications Ni and Pd have important roles and other combinations are relevant to a range of surface protection applications. Second, it is clear that the extent of metal penetration (seen here for Sn into Au but not Ag or Cu) is dependent on timescale. We therefore wish to look at shorter effective timescales for the mobile systems and at longer effective timescales for the apparently structurally static systems. According to circumstances, this might be effected directly or by altering film thickness. Third, for cases in which the data suggest the presence of lateral structural features, we suggest that off-specular NR measurements may be valuable.

As we pursue these future goals, we note that the STEP and QCM observations provide a very efficient means of exploring a wide range of parameter space (metals, concentrations,

electrochemical control function and associated potential/current, and timescale) in order to define the optimum conditions for the most informative NR experiment.

Conflicts of interest

There are no conflicts of interest to declare.

Funding Acknowledgements

KSR wishes to thank the European Union for funding under the Framework 7 programme for project ASPIS (**A**dvanced **S**urface **P**rotection for **I**mproved Reliability PCB **S**ystems Grant agreement no.: 243626). KSR also thanks Innovate UK (Manufacturing Electronic Systems of the Future) for funding under the MACFEST project (Project No: 102020). ERJP thanks the EPSRC and the University of Leicester for a studentship. RMS thanks the University of Leicester for a studentship. VCF thanks FCT for financial support (SFRH/BPD/77404/2011). We thank the ISIS Facility at the Rutherford Appleton Laboratory for provision of instrument time to make the NR measurements.

Figure legends

Figure 1. Schematic diagram of electrochemistry / NR cell; inset shows reflectivity at the interfaces within the system. (Adapted from ref. 34)

Figure 2. STEP experiment response for sequential metal stripping from Au(electrode)/Ag/Cu bilayer. Bilayer fabrication: AgCl (10 mM in Ethaline), deposited potentiostatically at -0.1 V (7200 s); Cu (10 mM in Ethaline), deposited potentiostatically at -0.6 V (7200 s). Galvanostatic stripping in Ethaline at i = 14.9 μA cm^{-2}. Other experimental details as in main text.

Figure 3. QCM / STEP experiment response for sequential metal stripping from AT-cut quartz/Au(electrode)/Ag/Cu bilayer. Bilayer fabrication: AgCl (20 mM in Ethaline), deposited potentiostatically at -0.1 V (1800 s); $CuCl_2$ (20 mM in Ethaline), deposited potentiostatically at -0.6 V (1800 s). Galvanostatic stripping in Ethaline at i = 51.6 μA cm^{-2}. Other experimental details as in main text. Panel a: QCM responses in air; b: QCM responses in Ethaline; c: overlaid STEP response and calculated mass change during stripping.

Figure 4. Raw NR profiles as functions of time during deposition (panel a) and stripping (panel b) of Au(electrode)/Ag/Cu bilayer. Bilayer fabrication: AgCl (10 mM in Ethaline), deposited potentiostatically at -0.4 V (10.8×10^3 s); $CuCl_2$ (10 mM in Ethaline), deposited potentiostatically at -0.4 V (21.6×10^3 s). Galvanostatic stripping in Ethaline at i = 14.3 μA cm^{-2}. Other experimental details as in main text. In panel a, the data for the two stages of the deposition are combined for presentational purposes.

Figure 5. Fitted NR profiles for the deposition (panel a) and stripping (panel b) of Au(electrode) /Ag/Cu bilayer; data from Fig. 4. In panel a, the data for the two stages of the deposition are combined for presentational purposes. Quantitative outcomes listed in Tables 1-4.

Figure 6. STEP experiment response for sequential metal stripping from Au(electrode)/Cu/Ag bilayer. Bilayer fabrication: $CuCl_2$ (10 mM in Ethaline), deposited potentiostatically at -0.6 V (7200 s); AgCl (10 mM in Ethaline), deposited potentiostatically at -0.4 V (7200 s). Galvanostatic stripping in Ethaline at i = 22.0 μA cm^{-2}. Other experimental details as in main text.

Figure 7. QCM / STEP experiment response for sequential metal stripping from AT-cut quartz/Au(electrode)/Cu/Ag bilayer. Bilayer fabrication: $CuCl_2$ (20 mM in Ethaline), deposited potentiostatically at -0.6 V (1800 s); AgCl (20 mM in Ethaline), deposited potentiostatically at -0.4 V (1800 s). Galvanostatic stripping in Ethaline at i = 57.9 µA cm^{-2}. Other experimental details as in main text. Panel a: QCM responses in air; b: QCM responses in Ethaline; c: overlaid STEP response and calculated mass change during stripping.

Figure 8. STEP experiment response for metal stripping from Au(electrode)/Sn layer. Layer fabrication: $SnCl_2$ (10 mM in Ethaline), deposited potentiostatically at -0.5 V (7200 s) Galvanostatic stripping in Ethaline at i = 19.1 µA cm^{-2}. Other experimental details as in main text.

Figure 9. Raw NR profiles as a function of time during deposition of Au(electrode)/Sn layer. Layer fabrication: $SnCl_2$ (10 mM in Ethaline), deposited potentiostatically at -0.4 V (21.6×10^3 s). Galvanostatic stripping in Ethaline at i = 14.3 µA cm^{-2}. Other experimental details as in main text.

Figure 10. STEP experiment response for sequential metal stripping from Au(electrode)/Ag/Sn bilayer. Bilayer fabrication: AgCl (10 mM in Ethaline), deposited potentiostatically at -0.1 V (7200 s); $SnCl_2$ (10 mM in Ethaline), deposited potentiostatically at -0.5 V (7200 s). Galvanostatic stripping in Ethaline at i = 19.3 µA cm^{-2}. Other experimental details as in main text.

Figure 11. STEP experiment response for sequential metal stripping from Au(electrode)/Cu/Sn bilayer. Bilayer fabrication: $CuCl_2$ (20 mM in Ethaline), deposited potentiostatically at -0.6 V (7200 s); $SnCl_2$ (20 mM in Ethaline), deposited potentiostatically at -0.5 V (7200 s). Galvanostatic stripping in Ethaline at i = 55.6 µA cm^{-2}. Other experimental details as in main text.

Tables

Layer	10^6 SLD / Å^{-2}	Thickness / Å		Roughness / Å		% Solvation	
		Value	±	Value	±	Value	±
MPTS	0.144	65.3	0.9	26.7	2.1	0*	-
Au	4.660	319.0	1.8	56.8	3.4	0*	-
Ag1	3.468	96.2	11.8	52.7	4.2	0.00	0.00
Ag2	3.468	155.8	1.5	52.7	3.4	0.00	0.00
Ag3	3.468	197.6	0.26	58.5	2.3	0.00	0.00
Ag4	3.468	235.9	4.4	60.5	2.9	0.00	0.00
Ag5	3.468	276.1	3.0	62.5	0.06	0.00	0.00
Ag6	3.468	304.2	1.9	61.3	3.3	0.00	0.00
Ag7	3.468	323.0	1.2	61.0	1.2	0.00	0.00
Ag8	3.468	349.4	4.8	62.0	3.1	0.00	0.00
Ag9	3.468	360.4	0.9	57.7	0.5	0.00	0.00
Ag10	3.468	384.6	1.3	56.2	2.8	0.00	0.00
Ag11	3.468	397.5	0.02	57.5	0.06	0.00	0.00
Ag12	3.468	416.5	3.6	60.7	0.6	0.00	0.00
Ag13	3.416	425.3	0.8	58.2	1.4	1.62	0.01
Ag14	3.468	439.9	6.3	63.1	3.8	0.00	0.00

Table 1. Fitted NR data (from Fig. 5) for potentiostatic deposition of Ag on Au. Sequence numbers (Ag1, …) represent sampled time slices during Ag deposition (see Fig. 5). Solvent content of MPTS and Au layers (marked *) set to zero.

Layer	10^6 SLD / $Å^{-2}$	Thickness / Å		Roughness / Å		% Solvation	
		Value	±	Value	±	Value	±
MPTS	0.144	68.6	1.1	26.5	1.9	0*	-
Au	4.660	315.8	3.8	48.1	2.2	0*	-
Ag	3.290	404.1	7.6	198.9	15.7	5.62	0.20
Cu1	4.240	1.00	0.07	70.2	4.1	36.6	2.6
Cu2	6.235	52.2	1.5	77.4	0.7	4.77	0.08
Cu3	6.388	101.6	5.8	85.7	3.5	2.33	0.01
Cu4	6.466	141.8	3.2	91.4	2.3	1.08	0.01
Cu5	6.504	182.0	1.9	95.4	4.5	0.47	0.00
Cu6	6.479	206.7	10.7	99.7	3.4	0.88	0.01
Cu7	6.431	224.1	2.8	100.2	0.85	1.64	0.01
Cu8	6.479	247.1	1.9	103.5	3.4	0.88	0.00
Cu9	6.505	267.4	0.5	106.5	4.2	0.47	0.00
Cu10	6.433	278.6	4.1	106.4	3.4	1.62	0.01
Cu11	6.493	296.4	4.0	109.3	5.0	0.66	0.01

Table 2. Fitted NR data (from Fig. 5) for potentiostatic deposition of Cu on Au/Ag. Sequence numbers (Cu1, …) represent sampled time slices during Cu deposition (see Fig. 5). Solvent content of MPTS and Au layers (marked *) set to zero.

Layer	10^6 SLD / Å^{-2}	Thickness / Å		Roughness / Å		% Solvation	
		Value	±	Value	±	Value	±
MPTS	0.144	69.0	1.1	24.5	1.4	0*	-
Au	4.660	318.9	2.2	55.0	0.03	0*	-
Ag	3.468	341.3	3.1	120.5	2.6	0.00	0.00
Cu1	5.996	279.8	8.3	149.0	13.4	8.58	0.21
Cu2	6.010	227.9	2.7	139.5	7.5	8.35	0.12
Cu3	5.999	207.8	2.2	124.2	3.9	8.53	0.18
Cu4	6.023	154.9	0.7	110.6	10.0	8.15	0.30
Cu5	6.317	121.8	6.3	113.9	6.6	3.46	0.09
Cu6	5.997	107.7	1.2	99.7	1.9	8.56	0.29
Cu7	6.147	74.8	1.7	108.6	6.1	6.17	0.26
Cu8	5.965	56.9	2.4	119.7	9.0	9.08	0.54
Cu9	5.877	28.1	3.5	116.8	6.5	10.48	1.00
Cu10	6.236	3.4	8.7	111.1	5.4	4.75	0.15

Table 3. Fitted NR data (from Fig. 5) for galvanostatic stripping of Cu from Au/Ag/Cu. Sequence numbers (Cu1, …) represent sampled time slices during Cu dissolution (see Fig. 5). Solvent content of MPTS and Au layers (marked *) set to zero.

Layer	10^6 SLD / Å^{-2}	Thickness / Å		Roughness / Å		% Solvation	
		Value	±	Value	±	Value	±
MPTS	0.144	69.0	5.9	24.5	6.8	0*	-
Au	4.660	318.9	2.0	55.0	0.02	0*	-
Ag1	3.468	292.9	8.0	96.7	7.0	0.00	0.00
Ag2	3.468	246.2	6.0	99.7	2.1	0.00	0.00
Ag3	3.468	220.4	2.5	106.7	3.4	0.00	0.00
Ag4	3.468	163.8	8.1	105.4	2.6	0.00	0.00
Ag5	3.329	93.3	3.2	81.9	3.8	4.33	0.14
Ag6	3.141	84.6	8.8	76.0	4.7	10.21	1.10
Ag7	3.150	48.3	4.6	71.7	4.5	9.93	0.99
Ag8	3.123	22.9	5.8	65.3	1.5	10.78	1.27
Ag9	3.106	20.2	1.1	62.8	1.7	11.30	1.12
Ag10	3.148	13.8	4.8	50.5	2.7	9.98	1.01

Table 4. Fitted NR data (from Fig. 5) for galvanostatic stripping of Ag from Au/Ag/Cu (subsequent to Cu stripping). Sequence numbers (Ag1, …) represent sampled time slices during Ag dissolution (see Fig. 5). Solvent content of MPTS and Au layers (marked *) set to zero.

References

[1] C. F. Coombs, *Printed Circuits Handbook*, McGraw-Hill, 5th edn., 2001.

[2] J. A. Scarlett, *Printed Circuit Boards for Microelectronics*, van Nostrand Reinhold Company Ltd., London, 1st edn., 1970.

[3] Karl Ryder, Andrew Ballantyne, Dennis Price and Tom Perrett, The PCB Magazine February 2015, 22.

[4] Robert Doering and Yoshio Nishi, Eds., "Handbook of Semiconductor Manufacturing Technology", 2nd ed., CRC Press, 2007,

[5] H. Yang, X. Guo, N. Birbilis, G. Wu and W. Ding, *Applied Surface Science*, 2011, **257**, 9094-9102

[6] J. P. Hallett and T. Welton, *Chemical Reviews*, **2011**, 111, 3508-3576.

[7] E. L. Smith, A. P. Abbott and K. S. Ryder, *Chemical Reviews*, **2014**, 114, 11060-11082.

[8] P. De Vreese, N. R. Brooks, K. Van Hecke, L. Van Meervelt, E. Matthijs, K. Binnemans and R. Van Deun, *Inorganic Chemistry*, **2012**, 51, 4972-4981.

[9] A. P. Abbott, K. El Ttaib, G. Frisch, K. J. McKenzie and K. S. Ryder, *Physical Chemistry Chemical Physics*, **2009**, 11, 4269-4277.

[10] A. R. Hillman, K. S. Ryder, C. J. Zaleski, V. Ferreira, C. A. Beasley and E. Vieil, *Electrochimica Acta*, **2014**, 135, 42-51.

[11] S. Ghosh and S. Roy, *Materials Science and Engineering B-Advanced Functional Solid-State Materials*, **2014**, 190, 104-110.

[12] S. Salome, N. M. Pereira, E. S. Ferreira, C. M. Pereira and A. F. Silva, *Journal of Electroanalytical Chemistry*, **2013**, 703, 80-87.

[13] A. P. Abbott, J. C. Barron and K. S. Ryder, *Transactions of the Institute Metal Finishing*, **2009**, 87, 201-207.

[14] M. Starykevich, A. N. Salak, D. K. Ivanou, A. D. Lisenkov, M. L. Zheludkevich and M. G. S. Ferreira, *Electrochimica Acta*, **2015**, 170, 284-291.

[15] J. Zhang, C. Gu, Y. Tong, J. Gou, X. Wang and J. Tu, *RSC Advances*, **2015**, 5, 71268-71277.

[16] E. S. C. Ferreira, C. M. Pereira and A. F. Silva, *Journal of Electroanalytical Chemistry*, **2013**, 707, 52-58.

[17] S. Fashu, C.-d. Gu, J.-l. Zhang, M.-l. Huang, X.-l. Wang and J.-p. Tu, *Transactions of Nonferrous Metals Society of China*, **2015**, 25, 2054-2064.

[18] A. P. Abbott, G. Capper, K. J. McKenzie and K. S. Ryder, *Journal of Electroanalytical Chemistry*, **2007**, 599, 288-294.

[19] F. Liu, Y. Deng, X. Han, W. Hu and C. Zhong, *Journal of Alloys and Compounds*, **2016**, 654, 163-170.

[20] A. Ballantyne, G. Forrest, M. Goosey, A. Griguceviciene, J. Juodkazyte, R. Kellner, A. Kosenko, R. Ramanauskas, K. S. Ryder, A. Selskis, R. Tarozaite and E. Veninga, *Circuit World*, **2012**, 38, 21-29

[21] S. Sigalov, N. Shpigel, M. D. Levi, M. Feldberg, L. Daikhin and D. Aurbach, *Anal. Chem.*, **2016**, 88, 10151-10157

[22] A. P. Abbott, M. Azam, K. S. Ryder and S. Saleem , *Anal. Chem.*, **2013**, 85, 6653-6660

[23] A. J. Goddard, R. C. Harris, S. Saleem, M. Azam, C. Hood, D. Clark, J. Satchwell and K. S. Ryder, *Trans. IMF*, **2017**, 95, 137-146.

[24] G. Pulletikurthi, M. S. Ghazvini, T. Cui, N. Borisenko, T. Carstens, A. Borodin and F. Endres, *Dalton Trans.*, **2017**, 46, 455-464

[25] A. P. Abbott, J. C. Barron, K. S. Ryder and E. L. Smith, *Anal. Chem.*, **2009**, 81, 8466-8471.

[26] J. Penfold, R. M. Richardson, A. Zarbakhsh, J.R.P. Webster, D.G. Bucknall, A. R. Rennie, R.A.L. Jones, T. Cosgrove, R. K. Thomas, J. S. Higgins, P. D. I. Fletcher, E. Dickinson, S. J. Roser, I. A. McLure, A. R. Hillman, R. W. Richards, E. J. Staples, A. N. Burgess, E. A. Simister and J.W. White, *Faraday Trans.,* **1997**, *93*, 3899-3917.

[27] A. R. Hillman, A. Glidle, R. M. Richardson, S. J. Roser, P. M. Saville, M. J. Swann and J. R. P. Webster, *J. Am. Chem. Soc*., **1998**, 120, 12882- 12890.

[28] A. R. Hillman, L. Bailey, A. Glidle, J. M. Cooper, N. Gadegaard and J. R. P. Webster, J. *Electroanal. Chem.*, **2002**, 532, 269-276.

[29] P. M. Saville, M. Gonsalves, A. R. Hillman and R. Cubitt, J. Phys. Chem. B, **1997**, 101, 1-4

[30] A. Glidle, J. Cooper, A. R. Hillman, L. Bailey, A. Jackson and J. R. P. Webster, *Langmuir*, **2003**, 19, 7746-7753.

[31] A. Glidle, L. Bailey, C. S. Hadyoon, A. R. Hillman, A. Jackson, K. S. Ryder, P. M. Saville, M. J. Swann, J. R. P. Webster, R. W. Wilson and J. Cooper, *Anal. Chem*. **2001**, 73, 5596-5606.

[32] A. Glidle, C. S. Hadyoon, N. Gadegaard, A. R. Hillman, K. S. Ryder, J. R.P. Webster, J. M. Cooper, R. W. Wilson and R. Cubitt, *J. Phys. Chem. B*, **2005**, 109, 14335-14343.

[33] J. F. K. Cooper, K. N. Vyas, N.-J. Steinke, D. M. Love, C. J. Kinane and C. H. W. Barnes, *Electrochimica Acta*, **2014**, 138, 56.

[34] Andrew D. Ballantyne, Robert Barker, Robert M. Dalgliesh, Virginia C. Ferreira, A. Robert Hillman, Emma J. R. Palin, Rachel Sapstead, Emma L. Smith, Nina-Juliane Steinke and Karl S. Ryder, J. Electroanal. Chem., 2018, (in press).

[35] NASF SURFACE TECHNOLOGY WHITE PAPERS 80 (5), 1-12 (February 2016), Simultaneous Thickness and Electrochemical Potential Determination of Individual Layers in Multilayer Nickel Deposits, by Edward P. Harbulak Chrysler Corporation Detroit, Michigan.

[36] E.P. Harbulak, Plating and Surface Finishing, **1980**, 67, 49-54.

[37] A.V. Hughes, RasCal. Sourceforge, Downloaded from: http://sourceforge.net/projects/rscl/, (2013) (2016).

[38] B. Efron, Bootstrap methods: another look at the jackknife, Ann. Stat. **1979**, 7, 1–26.

[39] A. P. Abbott, A. I. Alhaji, K. S. Ryder, M. Horne & T. Rodopoulos, Trans. IMF, **2016,** 94, 104-113.

Figure 1

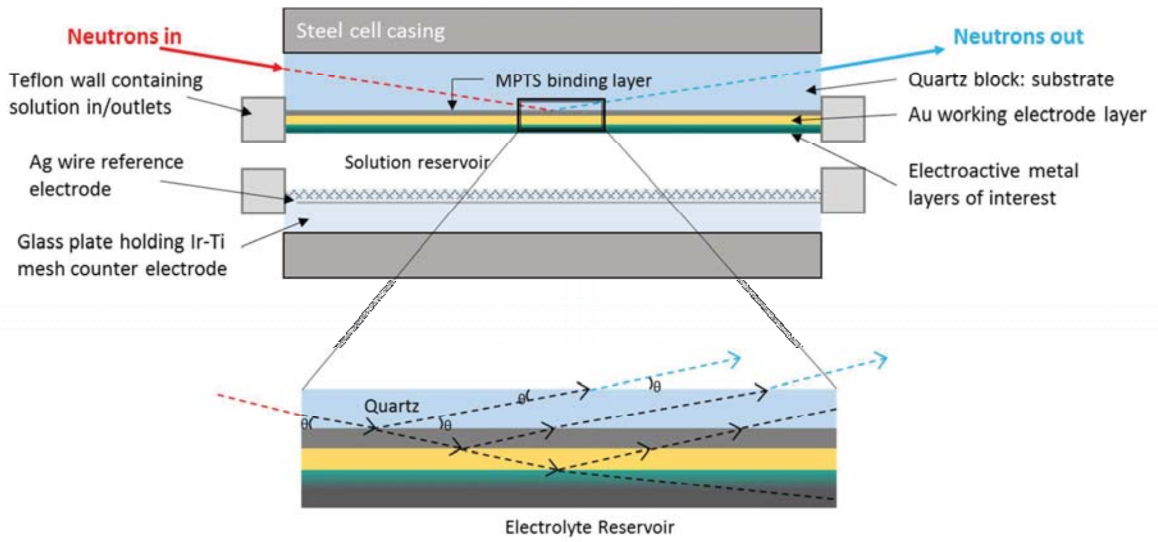

Figure 2

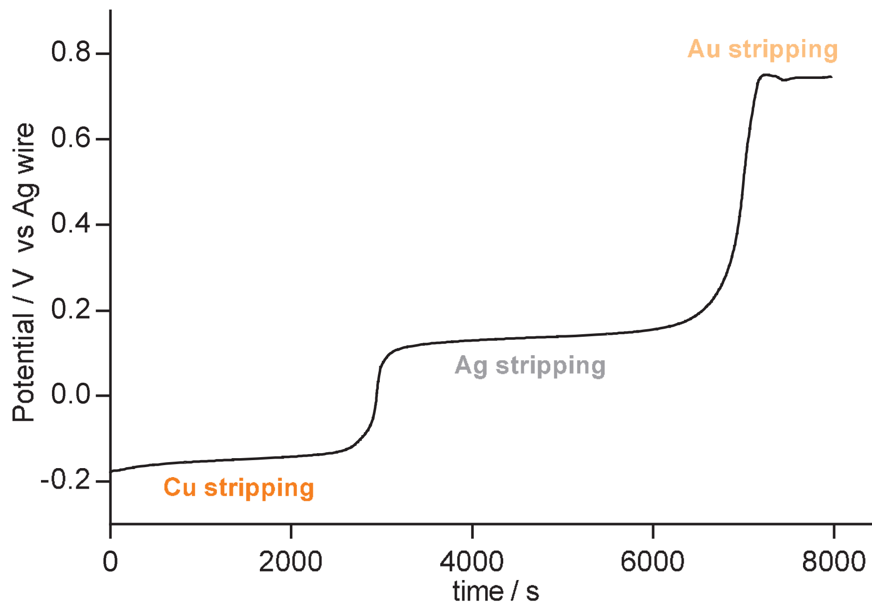

Figure 3

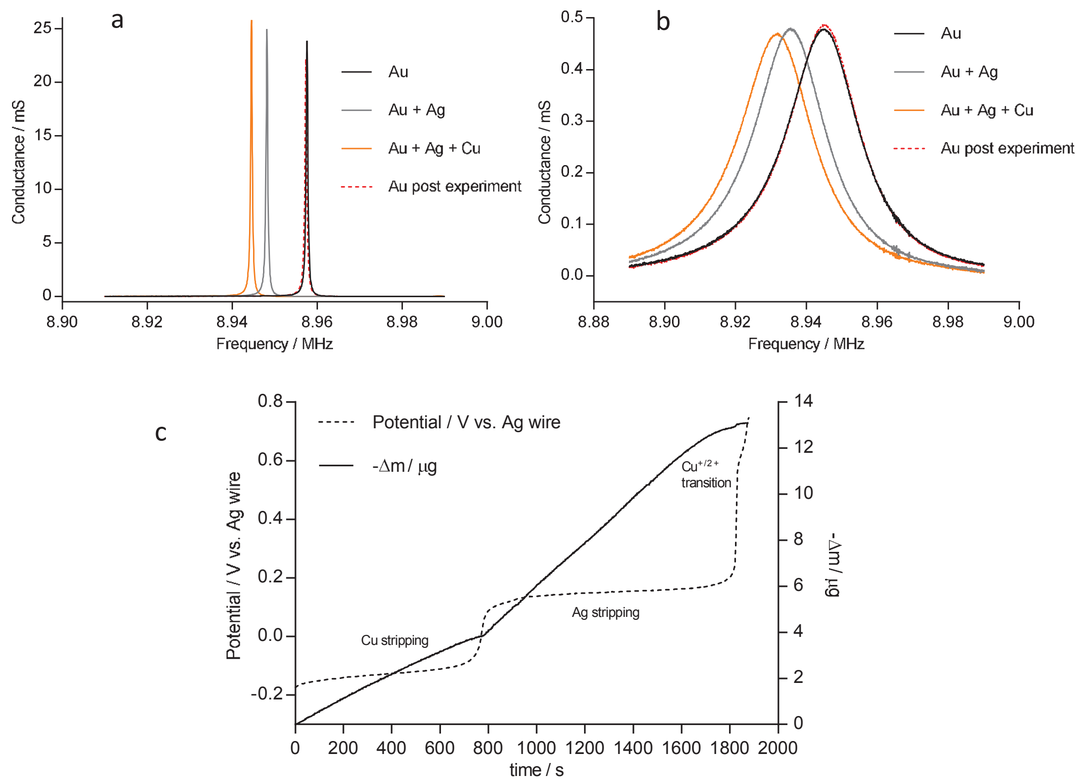

Figure 4

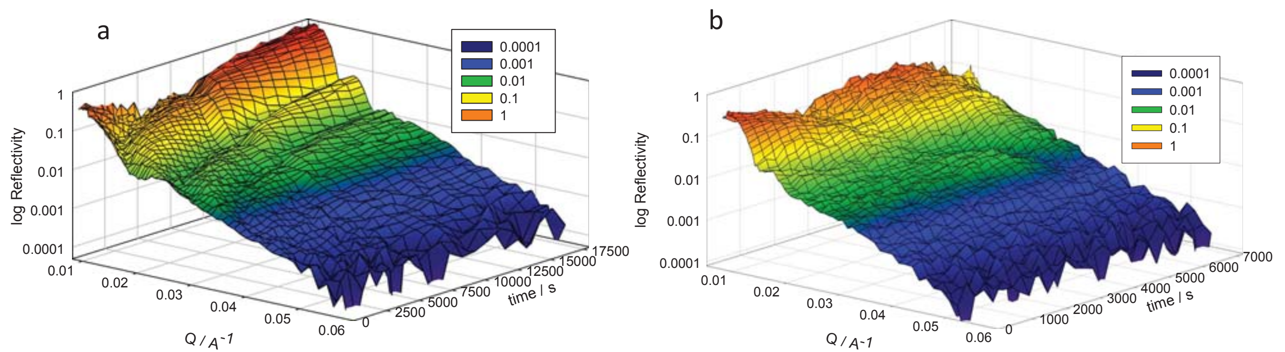

Figure 5

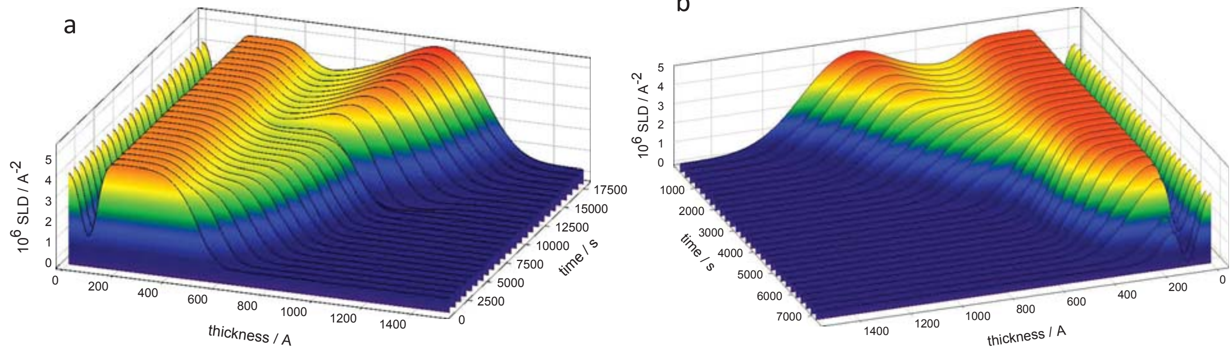

Figure 6

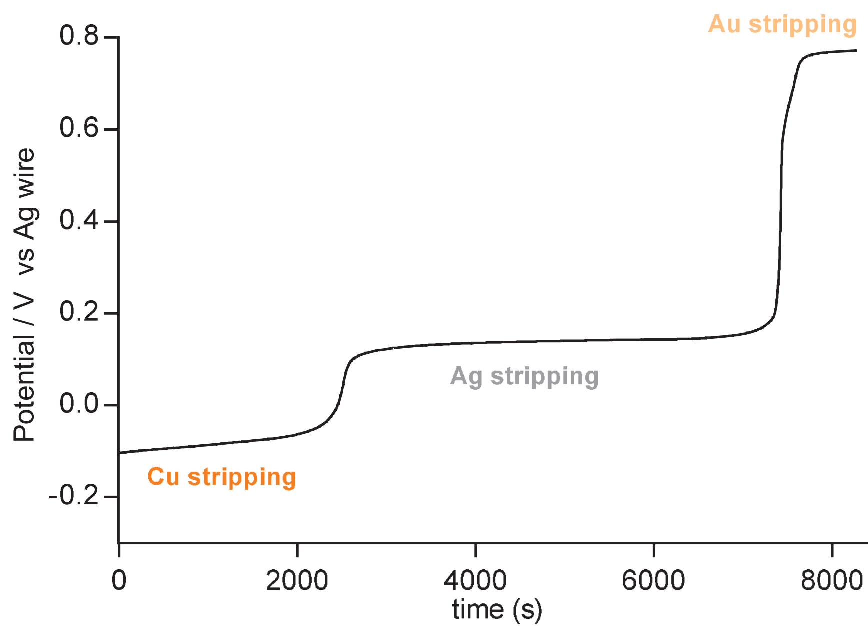

Figure 7

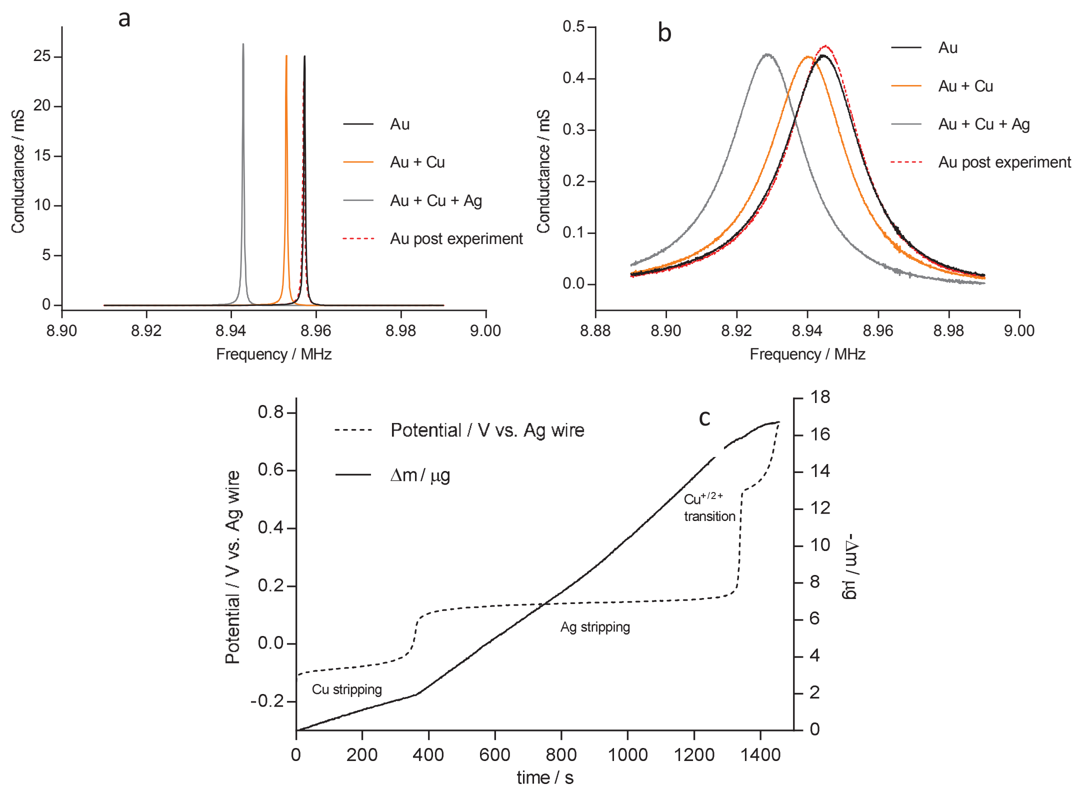

Figure 8

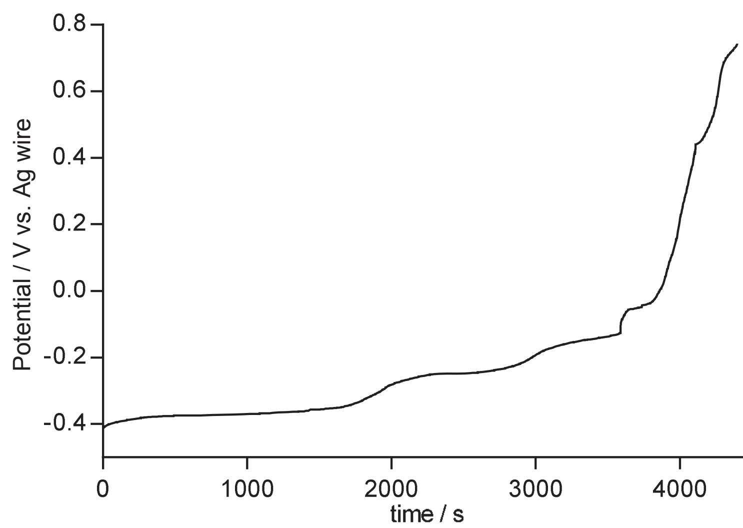

Figure 9

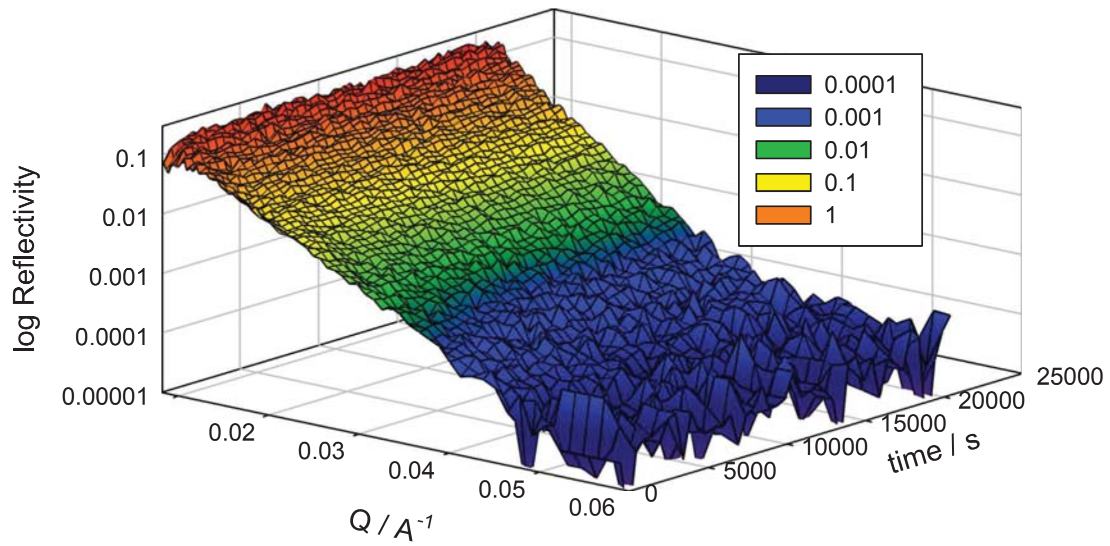

Figure 10

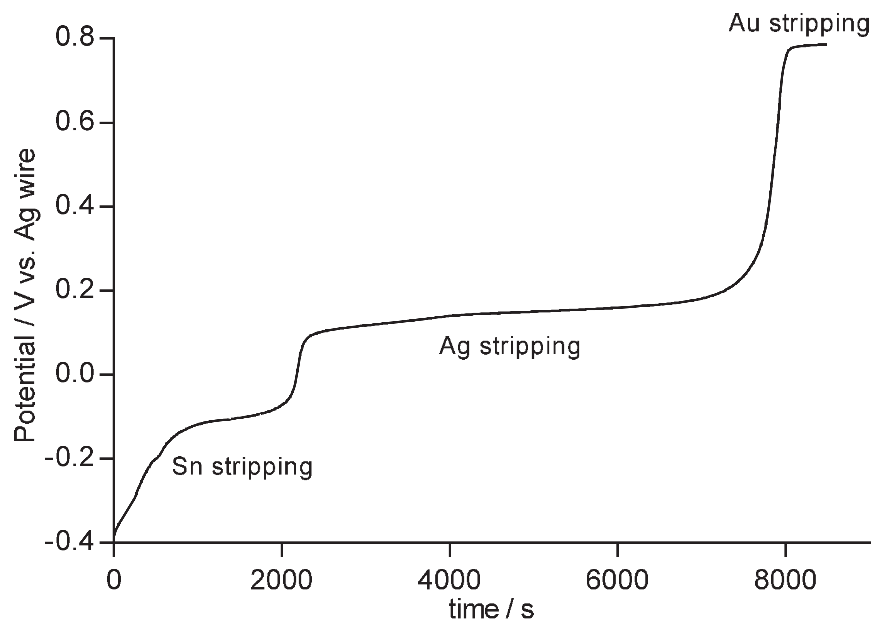

Figure 11